Biochimica et Biophysica Acta, 724 (1983) 433–446
Elsevier

BBA 41362

PHOTOACOUSTIC DETECTION OF PHOTOSYNTHETIC OXYGEN EVOLUTION FROM LEAVES

QUANTITATIVE ANALYSIS BY PHASE AND AMPLITUDE MEASUREMENTS

PATRICK POULET [a,b,*], DAVID CAHEN [a] and SHMUEL MALKIN [b,**]

Departments of [a] Structural Chemistry and [b] Biochemistry, The Weizmann Institute of Science, Rehovot 76100 (Israel)

(Received March 29th, 1983)

Key words: Oxygen evolution; Photosynthesis; Photoacoustic spectroscopy; (Tobacco leaf)

The photoacoustic signal from an intact leaf was analyzed as a vectorial summation of photothermal and photosynthetic oxygen-evolution contributions. A method is outlined to estimate each contribution separately. The amplitude of the oxygen-evolution component relative to that of the photothermal singnal decreases as the modulation frequency increases due to two processes which specifically damp the oxygen-evolution modulation: (1) diffusion of oxygen from the chloroplasts to the cell boundary, and (2) electron-transfer reactions occurring between the photochemical act and oxygen evolution. The effects of the two processes are well separated and are observed over different ranges of modulation frequency. Analysis of the data leads to a consistent estimation of the oxygen diffusion coefficient and also to a preliminary idea on the limiting time constant on the donor side of Photosystem II. The dependence of the photoacoustic oxygen-evolution signal on the intensity of added nonmodulated background light is used to construct the light saturation curve of (gross) photsynthesis, with an estimation of the ratio maximal rate/maximal quantum yield. The photoacoustic method is distinguished by its sensitivity and rapidity (a single measurement takes approx. 1 s), far better than any other method to measure gross photosynthesis. The only disadvantage is in the fact that the quantum yield of oxygen evolution is determined in a relative basis only. Attempts to calibrate the photoacoustic measurements in an absolute sense are underway.

Introduction

Photoacoustic measurements on intact leaves [1] provide quantitative information on two related aspects of the photosynthetic process, namely, photochemical energy storage and oxygen evolution. The total photoacoustic signal is the sum of two contributions:

(1) A photothermal one, resulting from partial or total conversion of the absorbed (modulated) light to modulated heat, which is then transduced to an acoustic wave [2].

(2) A direct photobaric one, due to modulated photosynthetic oxygen evolution, generated upon periodic excitation of the photosynthetic apparatus. In the following we will refer to this photobaric contribution also as the oxygen-evolution one.

Both contributions originate in the chloroplasts, from where heat and oxygen diffuse to the cell envelope, and generate acoustic waves in the air phase near the boundary of the cell. The photo-

* Present address: Institut de Physique Biologique, Faculté de Medicine, Université Louis Pasteur de Strasbourg, Strasbourg, France.

** To whom correspondence should be addressed.

thermal part of the photoacoustic signal is reduced by a fraction equal to that part of the photon energy which is stored by the photosynthetic process as chemical energy ('photochemical loss'). With the addition of sufficiently strong nonmodulated background light, which saturates photosynthesis by 'closing' the reaction centers, the modulated component of oxygen evolution and its resulting contribution to the photoacoustic signal are eliminated. At the same time, the photothermal contribution increases to its maximum level due to complete conversion of the absorbed modulated light to heat. The background light by itself does not contribute anything to the photoacoustic signal, as it is not modulated.

In previous reports we considered the photothermal and photobaric contributions to the photoacoustic signal as scalar quantities [1,3–5]. While this approach is oversimplified, it allowed us, nevertheless, to extract biologically relevant information on various leaf species. However, a complete description of the photoacoustic signal requires us to consider it as a vector sum of components, as can be understood by realizing that these components have different physical origins and, as such, can have different phase angles (cf. Appendix A).

Here we present an experimental and theoretical study of the oxygen-evolution vector as a function of the frequency and intensity of the background light. Comparing the phases of the oxygen evolution and photothermal contributions it is found that in the limit of very low frequencies their phases are not too different. In this case, when nonmodulated background light is applied, the simultaneous elimination of the oxygen-evolution contribution and the increase in the photothermal contribution produce together a net effect of decrease in the signal amplitude ('negative' effect). As the frequency increases the two effects may cancel each other in amplitude but not in phase. As the frequency increases still further the two signals are out of phase. In this case application of saturating nonmodulated background light may cause a net combined increase of the signal ('positive' effect) due to both the elimination of the oxygen-evolution component, and the genuine increase in the photothermal component. At still higher frequencies the oxygen-evolution component is damped completely, allowing measurement of pure photothermal signals. This explains quantitatively previous results [1].

The relative damping of the oxygen-evolution signal, compared to the photothermal signal, is explained (a) by the diffusion of oxygen from the chloroplasts to the gaseous phase and (b) by the electron-transport reactions occurring between the photochemical act and water splitting. Our data are used to estimate diffusion parameters for oxygen in the plant cell and limiting rate constants for reactions leading to photosynthetic oxygen evolution.

A further study was made of the dependence of the oxygen-evolution and photothermal signals on the nonmodulated background light intensity. This allowed us to make predictions with respect to the normal light saturation curve of photosynthesis.

Materials and Methods

Tobacco (*Nicotiana tabacum* var. Xanthi) was grown in a greenhouse. Leaves were harvested from a mature plant and kept in a beaker, half filled with water, until used in the following hours.

Photoacoustic measurements on leaves were performed as described previously [1]. The source for the measuring modulated light was a d.c. stabilized projector. The light passed through an appropriate filter and was modulated by a rotating wheel chopper, which produced equal periods with light on and light off. The nonmodulated background light came from a second projector, also operated on d.c., whose maximal intensity was approx. 300 W/m^2 (over a bandwidth of approx. 400–750 nm). Such intensity practically saturated oxygen evolution, as is shown in Results and Discussion. The description of the photoacoustic cell is detailed in Ref. 6.

In this work we were concerned with steady-state measurements only, hence they began after a certain transition period, during which the photoacoustic signal reached a constant steady-state value (cf. Ref. 1).

Separation and calculation of the oxygen-evolution and photothermal signals (cf. Appendix A and Fig. 1)

The signal was analyzed by a lock-in amplifier (Brookdeal 9502) in the two-phase mode, allowing

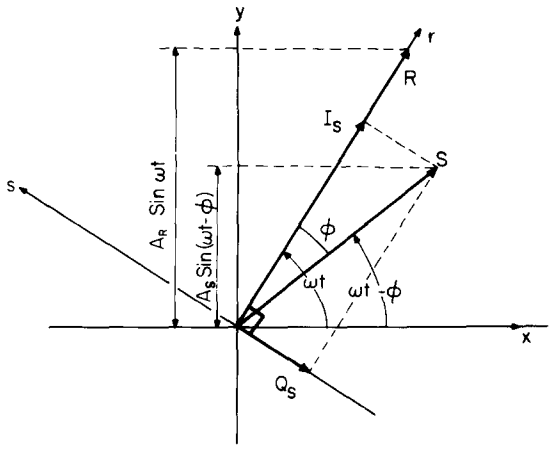

Fig. 1. A vectorial representation of sinusoidal signals. The (rotating) reference vector R produces a projection on the (fixed) y-axis equal to $A_R \sin \omega t$ while the (rotating) signal vector S produces a projection equal to $A_S \cos \phi \sin \omega t - A_S \sin \phi \cos \omega t$. The constant coefficients of this expression are, respectively, the projections of S on the (rotating) axes r and s (in-phase and quadrature).

simultaneous recording of the in-phase and quadrature (90° out-of-phase) components of the signal. In some experiments the phase angle with respect to the instrumental reference was adjusted in the instrument so as to have a zero-quadrature signal when only a true photothermal contribution existed (i.e., in the presence of saturating background light). The photothermal contribution is thus adjusted to appear only as an in-phase component. When the background light is switched off the resulting quadrature signal is due to oxygen evolution only. (The in-phase signal is still a mixture of photothermal and oxygen-evolution contributions).

For any arbitrary setting of the reference signal, the in-phase (I) and quadrature (Q) components are given by:

$$I = I_{th}(1-L) + I_{ox}$$

$$Q = Q_{th}(1-L) + Q_{ox} \qquad (1)$$

where the subscripts th and ox represent thermal and oxygen-evolution contributions, respectively. L is the 'photochemical loss' [7,8] in the photothermal contribution. When a saturating, nonmodulated, background light is applied, these components are:

$$I^* = I_{th}$$

$$Q^* = Q_{th} \qquad (2)$$

where the asterisk denotes the presence of saturating background light. Therefore, the change in the signal upon application of the saturating background light is obtained by vectorial subtraction:

$$-\Delta I = I - I^* = I_{ox} - LI_{th} = I_{ox} - LI^*$$

$$-\Delta Q = Q - Q^* = Q_{ox} - LQ_{th} = Q_{ox} - LQ^* \qquad (3)$$

At sufficiently high frequency the oxygen-evolution contribution can be neglected entirely. Then:

$$\Delta I' = LI'_{th} = LI'^*$$

$$\Delta Q' = LI'_{th} = LQ'^* \qquad (4)$$

where the primes denote the high-frequency case. L is then evaluated from the ratios $\Delta I'/I'^*$ or $\Delta Q'/Q'^*$:

$$L = \Delta I'/I'^* = \Delta Q'/Q'^* = \Delta A'/A'^* \qquad (5)$$

where A is the absolute value (amplitude) of the total vector signal.

It should be noted that the above equations are based on the assumption that practically no change of phase angle occurs in the photothermal signal when the background light is applied. This was verified experimentally in the high-frequency limit for photopacoustic measurements, as reported here, and also at low frequency by direct photothermal radiometry measurements, reported in Ref. 5.

If L is frequency independent then the L value, obtained by use of Eqn. 5, can be used in Eqn. 3 in order to find I_{ox} and Q_{ox}:

$$I_{ox} = I - (1-L)I^*$$

$$Q_{ox} = Q - (1-L)Q^* \qquad (6)$$

If L is frequency dependent it would be necessary to measure it at the same frequency by a different method, viz., infrared photothermal radiometry [5] and substitute the measured value of L in Eqn. 6.

From Eqn. 6 one can calculate the amplitude and phase angle of the oxygen-evolution vector: $A_{ox} = \sqrt{I_{ox}^2 + Q_{ox}^2}$ and $\phi_{ox} = \arctan(-Q_{ox}/I_{ox})$,

respectively. These are compared to the photothermal signal of amplitude $A_{th} = \sqrt{I_{th}^2 + Q_{th}^2}$ and phase angle $\phi_{th} = \arctan(-Q_{th}/I_{th})$. We were mainly concerned with the ratio of amplitudes (A_{ox}/A_{th}) and phase angle difference $\Delta\phi = (\phi_{ox} - \phi_{th})$.

Results and Discussion

Phase angle changes upon application of saturating background light

Examples of raw data are given in Fig. 2A. Fig. 2B is a representation of the same data showing the (computed) differences in phase angle (ϕ) and amplitude (A) of the vector signal upon application of background light.

When only a photothermal contribution is present there is no change in the phase angle of the signal vector when a saturating background light was applied. Such is the case for very-high-frequency photoacoustic measurements (Fig. 2, 480 Hz data) and was observed previously when performing infrared photothermal radiometry measurements [5] over the range of frequencies where this particular method could be used (3–100 Hz).

This is not the case, however, for lower frequency photoacoustic measurements, as is demonstrated in Fig. 2. Here, a considerable phase change may accompany the amplitude change upon application of the background light, especially in an intermediate range of frequencies where the amplitude changes are relatively small. This is consistent with our concept that the photoacoustic signal contains two contributions which have different phase angles (viz., photothermal and oxygen evolution of which one is eliminated completely when the background light is applied.

Frequency dependence of the oxygen-evolution and photothermal signals

Analyzing the signals as described in 'Materials and Methods' leads to a separate estimate of the photothermal and oxygen-evolution parts.

Data obtained in experiments, similar to those shown in Fig. 2, were collected at various frequencies. Table I illustrates the computation of photothermal and oxygen-evolution signals. In the present investigation the 'photochemical loss', L, was estimated as the high-frequency limit of the change of the signal amplitude induced by the back-

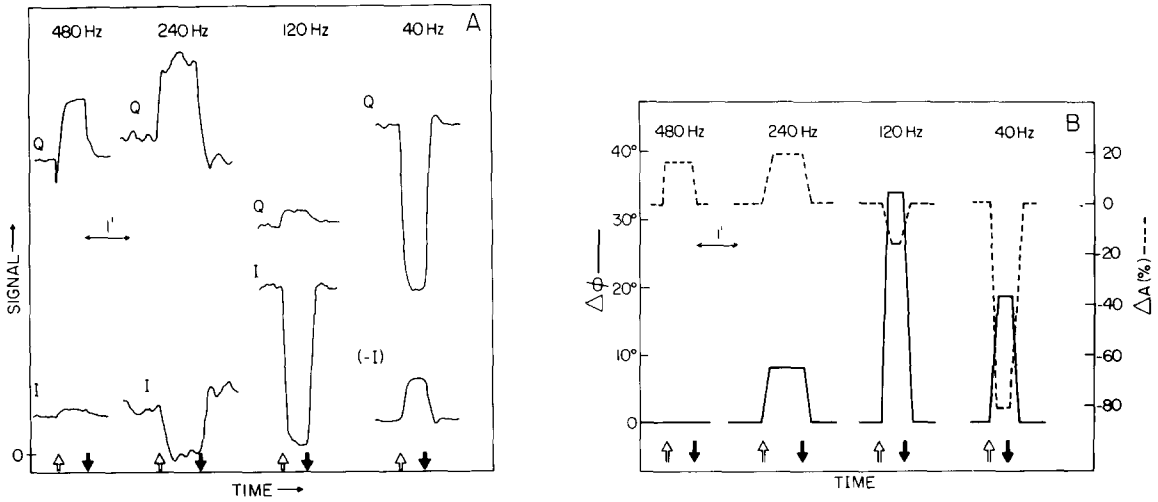

Fig. 2. (A) Raw data for the photoacoustic in-phase (I) and quadrature (Q) components from an active tobacco leaf, and their change as a saturating background light is applied (⇑, background light on; ⇓, background light off). The zero level is the same for both I and Q. The modulation frequencies are indicated at the top of the figure. I at 40 Hz has a negative magnitude. The reference phase angle was chosen in an arbitrary way. (B) The amplitude (ΔA, ———) and phase ($\Delta\phi$, — — —) changes of the photoacoustic signal, upon application of the background light signal, calculated from the raw data of panel A. Note that the sensitivity is different for the different frequencies. The change of amplitude is in percent, relative to the amplitude of the maximal photothermal signal alone (i.e., the photoacoustic signal in the presence of saturating background light).

TABLE I

AN EXAMPLE FOR THE ANALYSIS OF RAW DATA TO ESTIMATE THE PHOTOCHEMICAL LOSS, OXYGEN EVOLUTION AND PHOTOTHERMAL SIGNALS

Signal components are expressed in arbitrary but consistent units (mV), as measured at the input of the lock-in amplifier (after preamplifiation). Phase angles are expressed in degrees . r, raw data; c, calculated.

		Frequency (Hz)	
		480	60
I	(r)	0.95	22
Q		6.70	96
A	(c)	6.77	98.5
ϕ		82	77
$I^* = I_{th}$	(r)	1.10	−10
$Q^* = Q_{th}$		8.10	60
$A^* = A_{th}$	(c)	8.17	61
$\phi^* = \phi_{th}$		82	99.5
L	(c)	0.17	0.17 [b]
I_{ox}	(c)	0 [a]	30
Q_{ox}		0 [a]	46
A_{ox}	(c)	0	55
ϕ_{ox}		0	57
A_{ox}/A_{th}	(c)	0	0.90
$\Delta\phi = \phi_{ox} - \phi_{th}$		-	−42.5

[a] Assumed.

[b] Assumed to be equal to the L value at 480 Hz.

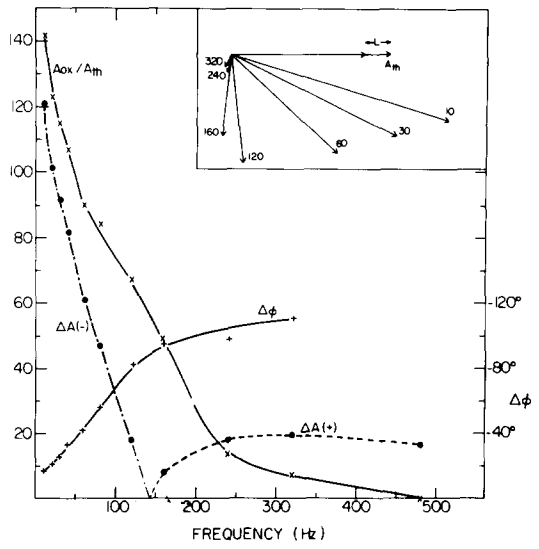

Fig. 3. The relation of the oxygen-evolution signal and phothermal signal at various modulation frequencies. (× ——— ×) The ratio of amplitude A_{ox}/A_{th} (in %); (+ ——— +) the phase angle difference $\Delta\phi$ between the oxygen and the photothermal signals; (●— — —●) the (calculated) change in amplitude (in %) of the total signal upon application of saturating background light. $\Delta A(-)$ is the negative effect (decrease in total amplitude) and $\Delta A(+)$ the positive effect (increase in total amplitude). The extent of the signal in the presence of the saturating background light is taken as unity. (Inset) Vectorial diagram of the photothermal signal (A_{th}) and the oxygen signal (all the other arrows) at various frequencies. The maximal photothermal signal is normalized to the same value at any frequency, and serves as a reference to the oxygen signals at various frequencies (denoted by the numbers in Hz). The photochemical loss in the photothermal signal is indicated by L. The photoacoustic signal can be found from a vectorial summation of ($A_{th} - L$) and each one of the oxygen signals.

ground light relative to the amplitude of the signal under strong background illumination. The value obtained was about 17%. This value of L has been used to calculate the oxygen signal, at various frequencies. Fig. 3 shows the results of calculations of the oxygen vector signal, relative to the (maximal) photothermal signal. With increasing frequency the ratio of amplitudes, A_{ox}/A_{th}, decreases while the phase angle difference between the two vectors increases. This is illistrated in a more pictorial way by the vector diagram in the inset, where both the photothermal and oxygen-evolution signals are represented by their vectors showing their amplitude and direction, at various frequencies. In this diagram the photothermal vector is always normalized to be same amplitude and direction. It is seen that at sufficiently low frequencies (approx. 20 Hz) the vectors have nearly the same direction. In this case the relatively large oxygen-evolution signal adds to the thermal signal and the net effect of the background light on the amplitude is to decrease it (negative effect). As the frequency increases, the oxygen-evolution signal is damped and delayed compared to the thermal signal, its elimination by the background light produces a decreasing negative effect on the total amplitude. The negative effect cancels the positive effect of the photochemical loss at some intermediate frequency (about 150 Hz) so that then the net effect on the amplitude is zero. At higher

frequencies the oxygen-evolution signal has an opposite directional sense and this leads to a positive background light effect on the total amplitude which adds to the positive effect due to the photochemical loss. At still higher frequencies the oxygen-evolution signal is fully damped and the effect of the background light is due only to the loss of modulated photochemical activity. This behavior qualitatively explains why, in amplitude measurements, the extent of the positive effect as a function of frequency (cf. also Fig. 3 in Ref. 1.) goes through a maximum and then tends to a lower steady-state value as the frequency increases. In Fig. 3 of Ref. 1 this behavior can be seen very clearly and the maximum in the total amplitude is very pronounced.

Damping of the modulated oxygen-evolution signal at high frequencies due to diffusion and limiting reaction steps

The oxygen-evolution and photothermal components of the photoacoustic signal originate at a common site, viz., the chloroplast pigments. Heat and oxygen diffuse out from the chloroplasts through the cell and both are transduced to an acoustic wave at the inner air phase near the boundary of the cell. The modulated temperature and oxygen concentration fields at their common source are proportional to each other (being both proportional to the exciting modulated light intensity) and they share common diffusion paths.

As a first approximation one can deal with a certain average diffusion path length, l, from the chloroplasts to the cell boundary. The chloroplasts in the cell are usually arranged in a concentric manner near the periphery of the cell; the closest distance to the cell boundary is of the order of 1 μm. The diffusion equation for oxygen in this case, assuming a one-dimensional model, was dealt with in Ref. 1. The most relevant result is that the amplitude of the modulated oxygen concentration field is attenuated at a distance x from the source by $\exp(-\sqrt{\omega/2D_{ox}}\cdot x)$ and therefore its value at the boundary is proportional to $\exp(-\sqrt{\omega/2D_{ox}}\cdot l)$. Here ω is the angular frequency (rad/s), equal to $2\pi f$ (f is the frequency in Hz) and D_{ox} is the diffusion coefficient of oxygen in the aqueous medium of the cell. The temperature field obeys a completely analogous diffusion equation, with a different diffusion coefficient (diffusivity) D_{th}, equal to $\kappa/c\rho$, where κ is the heat conductivity, c the heat capacity and ρ the density of the cell medium. In an analogous manner to the behavior of the oxygen concentration field, the modulated temperature field is attenuated at the cell boundary by $\exp(-\sqrt{\omega/2D_{th}}\cdot l)$.

In addition to the diffusion effect, the oxygen-evolution signal is already damped at the source by kinetic factors due to the chain of electron-transport reactions between the photochemical reaction and the step of oxygen formation [1]. If first-order reactions are assumed then for each reaction step, having a rate constant k_i, a simple theory predicts an attenuation factor of the form $k_i/\sqrt{k_i^2+\omega^2}$. This factor tends to unity at frequencies well below k_i. The total attenuation of the oxygen-evolution signal is the product of such factors.

One expects a linear relation between the periodic pressure changes (acoustic wave) and both the value of the modulated oxygen concentration and the modulated temperature at the boundary of the cell. The coefficients of this transduction depend on the parameters of the photacoustic chamber, the inner geometry of the leaf, the ambient physical conditions and also have the same frequency dependence (ω^{-1}). Thus, in the ratio of the amplitudes (oxygen-evolution signal : photothermal signal) the dependency on the frequency due to the transduction to an acoustic signal is eliminated and this ratio depends directly on the specific attenuation factors considered above. Therefore:

$$\frac{A_{ox}}{A_{th}} = \exp\left[-\sqrt{\pi f}\left(1/\sqrt{D_{ox}} - 1/\sqrt{D_{th}}\right)l\right] \cdot k_1/\sqrt{k_1^2+4\pi^2f^2}\cdot k_2/\sqrt{k_2^2+4\pi^2f^2}\ldots \qquad (7)$$

A plot of $\ln A_{ox}/A_{th}$ vs. $\sqrt{f}$ should tend to a straight line at sufficiently low frequencies (such that $f \ll k_i$) having a slope $-\sqrt{\pi}\,l\,(1/\sqrt{D_{ox}} - 1/\sqrt{D_{th}})$ from which D_{ox} can be computed, assuming reasonable values for l and D_{th} ($1/\sqrt{D_{th}}$ can usually be neglected, as compared with $1/\sqrt{D_{ox}}$, and omitted from Eqn. 7, resulting in a simplified equation with a corresponding slope $-\sqrt{\pi/D_{ox}}\,l$).

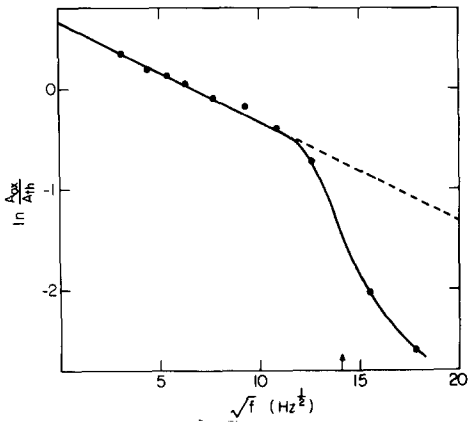

Fig. 4. A plot of $\ln A_{ox}/A_{th}$ vs. the square root of the frequency (cf. Eqn. 7). The arrow on the abscissa indicates the point where the second attenuation (due to electron-transport reactions) is half maximum (from the same data as those shown in Fig. 3).

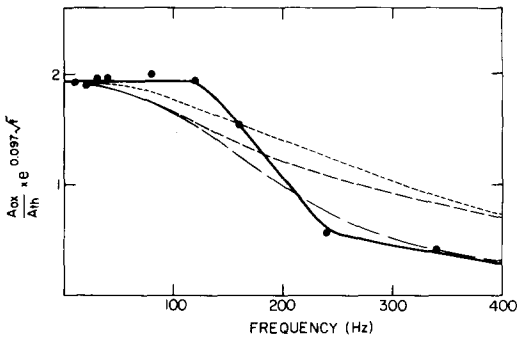

Fig. 5. A plot of $A_{ox}/A_{th} \cdot \exp(0.097\sqrt{f})$ vs. the frequency f, to emphasize the attenuation due to intermediate reactions (solid curve). The dashed curves represent examples for calculated attenuation factors: (middle) a single attenuation factor of the form $k_i/\sqrt{k_i^2+4\pi^2 f^2}$ with $k_i = 1000\ s^{-1}$; (top) a product of two attenuation factors having the same k_i ($= 2000\ s^{-1}$); (bottom) a product of four attenuation factors having the same k_i ($= 2000\ s^{-1}$).

Deviations from this line, at higher frequencies, can yield estimates of the k_i.

Such a plot is shown in Fig. 4. Indeed, the low-frequency part of the curve can be approximated by a straight line over a considerable range. The measured value of the slope is $-0.097\ s^{1/2}$. Assuming a mean path of diffusion of 10^{-4} cm and a thermal diffusivity as in pure water ($1.44 \cdot 10^{-3}\ cm^2 \cdot s^{-1}$), this slope corresponds to a diffusion coefficient for oxygen inside the cell, D_{ox}, of about $3.7 \cdot 10^{-6}\ cm^2 \cdot s^{-1}$ ($3.3 \cdot 10^{-6}$, in the same units, if the reciprocal thermal diffusivity is neglected). This value, although one order of magnitude smaller than that of D_{ox} in pure water ($2.1 \cdot 10^{-5}$ in the same units – handbook datum), is quite reasonable, considering the much higher cytoplasm viscosity. Another example of estimating oxygen diffusion in a living cell, by a completely different methodology, is quoted in Ref. 9 and leads to an even smaller value. Large differences between individual cells are expected due to the large variability of the plasma viscosity. Also, since the value of l was taken somewhat arbitrarily only order of magnitudes for D_{ox} can be obtained.

The large additional attenuation of the oxygen-evolution signal, relative to the thermal signal, in the frequency range above about 120 Hz, must be attributed to the reaction steps leading to oxygen evolution. This form of attenuation is best demonstrated by eliminating that attenuation which is due to diffusion. This is done by multiplying the ratio A_{ox}/A_{th} by $\exp(0.097\sqrt{f})$, which is the reciprocal of the experimental diffusional attenuation factor, and plotting this vs. the frequency (Fig. 5). As Fig. 5 shows, this second attenuation mechanism leads to a considerable further reduction of the signal at high frequencies, by factor of two at about 200 Hz. This particular point corresponds to a rate constant ($k_i = \frac{2\pi f}{\sqrt{3}}$) of about 700 s^{-1}, if only one attenuation factor of Eqn. 7 is considered. However, the attenuation curve of Fig. 4 is very sharp and quantitatively not consistent with a single factor of the form $k_i/\sqrt{k_i^2+\omega^2}$. For comparison, this theoretical relation is represented also in Fig. 5. We tried to obtain a better agreement between theory and experiment by considering products of the above attenuation factors. This leads to some improvement (cf. for examples in Fig. 5), but good agreement of both low- and high-frequency ranges could not be obtained with first-order reactions. The attenuation mechanism must therefore be reconsidered by replacing the simple model of consecutive first-order reactions, as done in Ref. 1, by a more sophisticated model. In any case the rate constant quoted above, or those computed according to a combination of several attenuation factors, agree in order of magnitude with limiting rate constants as estimated elsewhere [10], and can be taken as a crude first approximation.

The relation of photoacoustic oxygen-evolution measurements to the ordinary rate measurements of photosynthesis

In this section, we will show how to conduct and analyze photoacoustic oxygen-evolution measurements which will yield direct information on the ordinary rate and quantum yield of photosynthesis. The photoacoustic measurements are ordinarily carried out under limiting light conditions, and the ratio of A_{ox} to the light intensity is proportional to the quantum yield. One may introduce, however, various additional levels of non-modulated background light, each resulting in a certain average (steady) light intensity I_s. This will cause A_{ox} to decrease, due to a lowered quantum yield of oxygen production. The dependence of the oxygen-evolution component of the photoacoustic signal on I_s is related to the ordinary light saturation curves of photosynthesis (viz., the rate, r_s, vs. I_s) and indirectly gives information on the maximal rate. This is shown in the following analysis:

From the ordinary light saturation curves of photosynthesis (Fig. 6) one can define two kinds of quantum yield, at each point of the light saturation curve: The integral (or ordinary) quantum yield γ_i is simply the ratio: rate/(absorbed) light flux (mol/E), i.e., r_s/I_s. The differential quantum yield γ_d is equal to the ratio: change of rate/change of absorbed light flux, i.e., dr_s/dI_s. Both definitions give, of course, the same value for the initial linear part of r_s vs. I_s, which is the maximal quantum yield.

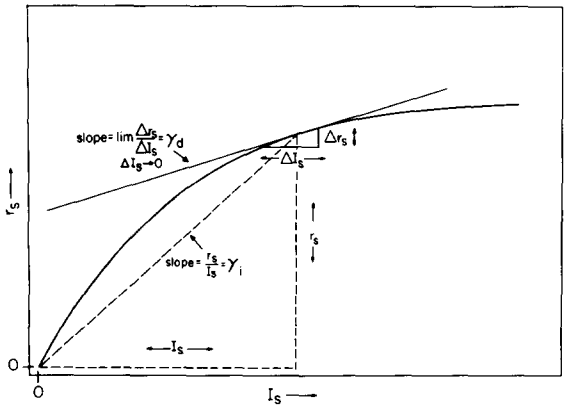

Fig. 6. Theoretical representation of the light saturation curve of photosynthesis (r_s vs. I_s) with the definitions of the integral (γ_i) and differential (γ_d) quantum yields represented, respectively, by the slope of the chord drawn between the origin and a given point on the curve, and by the slope of the tangential line at the same point.

It can be shown (cf. Appendix B), and is also intuitively conceivable, that at sufficiently low frequency the light modulation in the photoacoustic experiment is slow enough so that during each on and off period of the modulated light the photosynthetic system adjusts itself completely to the varying light intensity. If this is the case then the rate oscillates exactly according to the light saturation curve, around an average point fixed by I_s. If the intensity of the modulated light, i, is small enough, the amplitude of the rate oscillation is given approximately by $(dr_s/dI_s)i$, i.e., $\gamma_d i$. Thus, the ratio of the oxygen-evolution component of the photoacoustic signal to the modulated light intensity amplitude (if sufficiently small) is proportional to the differential quantum yield.

It is shown also (cf. Appendix B) that at sufficiently high frequency the photosynthetic system cannot adjust itself to the rapid fluctuations. The reaction centers respond only to the average background light intensity I_s and the extent of their closure determines a certain fixed quantum yield (r_s/I_s). The rate will fluctuate according to the fluctuations of the light intensity only, and its amplitude will be given by $(r_s/I_s)i$. In this case the oxygen-evolution component of the photoacoustic signal will measure the integral quantum yield.

The most usable analytical rate expression for gross photosynthesis for a homogeneous preparation is of the form (cf. also Appendix B, Eqn, B-5a):

$$r_s = \frac{\Phi r_{max} I_s}{\Phi I_s + r_{max}} \tag{8}$$

where r_{max} is the maximal saturation rate and Φ the maximal quantum yield, obtained under limiting light conditions. For the above expression γ_i and γ_d take the following forms (cf. Appendix B, Eqns. B-6 and B-7):

$$\gamma_i = \frac{\Phi r_{max}}{\Phi I_s + r_{max}}$$

$$\gamma_d = \frac{\Phi (r_{max})^2}{(\Phi I_s + r_{max})^2} \tag{9}$$

Thus, we expect that at very low frequencies a plot of the square root of the inverse of A_{ox} (or any of its vectorial components) vs. I_s will give a straight line. Most conveniently a relative value of A_{ox} should be used by normalizing its value at $I_s = 0$ to 1. In this case the slope would be equal to Φ/r_{max} (and the intercept to 1). Such a plot therefore gives information on r_{max} provided that Φ is known. We hope, in the future, to achieve an absolute quantitation of Φ directly from photoacoustic measurements. Here we will assume plausible values for Φ to make a preliminary estimate of r_{max}.

The above predictions were checked experimentally for low-frequency photoacoustic measurements. Fig. 7 presents experimental results for three different cases in all of which the plots of $1/A_{ox}$ vs. I_s are indeed linear. For the purpose of expressing r_{max} in terms of equivalents of O_2 evolved per unit time, we will equate I_s with the measured incident light flux (this is the average rate of light absorption per unit area), assuming that practically all the incident light is absorbed (ignoring losses from reflected and transmitted light). The use of such a simple average rate of light absorption is not obvious, in view of the expected variations of light intensity with leaf depth. However, the heterogeneity in the light

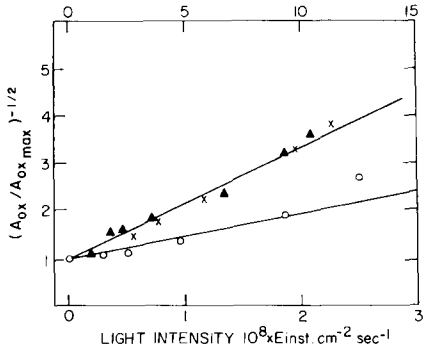

Fig. 7. A plot of the normalised inverse of the square root of the oxygen signal vs. the background light intensity, as according to Eqn. 9b. (×) Data for modulated light of broad wavelength bandwidth (400–600 nm) of intensity 7.8 W/m^2 (approx. $3 \cdot 10^{-9}$ E·cm^{-2}·s^{-1}). Background light 400–750 nm; (▲) data for modulated light of 590–660 nm, intensity 11 W/m^2 (approx. $6 \cdot 10^{-9}$ E·cm^{-2}·s^{-1}). Background light 400–750 nm; The light intensity scale for the above two sets of experiments is indicated at the top. (○) Data for modulated light of 590–660 nm, intensity 11 W/m^2. Background light 400–600 nm. Light intensity scale is indicated at the bottom.

energy density throughout the leaf may be much less severe than that considered by a simple Beer-Lambert law of light attenuation for the case of continuous distribution of pigments: multiple scattering and free passage through unpigmented sections tend to smooth out any directed light attenuation in the path of the incident light. Thus, as a rough first approximation the above average rate of light absorption may serve our purpose.

Analysis of Fig. 7, in view of the above, results in the following estimations of r_{max}/Φ for the three experimental cases; 43, 43 and 22 nmol O_2/cm^2 leaf area per s. Using a conventional value of Φ (= 0.1), these values correspond to maximal rates, expressed in more familiar units, of about 15, 15 and 8 mol $O_2 \cdot cm^{-2} \cdot h^{-1}$. To express these rates on a chlorophyll basis we measured the total chlorophyll (Chl) density by the usual extraction and spectroscopic estimation [11], which gave approx. 40 mg Chl/cm^2. From this the estimated rates per chlorophyll are about: 380, 380 and 200 mol O_2/mg Chl per h. The first two values are probably overestimated by the fact that for these experiments white light was used and part of the recorded light intensity was therefore in the inactive infrared. The third experiment in which a narrower wavelength band was used seems therefore more accurate. The estimated rate(s) are in the usual range of values for photosynthetic rates [12].

The above approach for using photoacoustics to estimate photosynthetic parameters will be perfected in further work when it will be possible also to estimate the absolute value of Φ, independently. This task seems possible in principle, using the ratio of the oxygen-evolution component to the photothermal one.

In conclusion, the photoacoustic method proves to yield rich information on the photosynthetic apparatus of intact leaves. Part of this information is not accessible by other methods (e.g., energy storage, diffusion parameters, etc.). The photosynthetic saturation curve is obtained rapidly and easily by the photoacoustic method, simply by continuous and fast variation of the background light intensity. Moreover, the rapidity of the measurement allows a continuous monitoring of fast transients and transitions to various physiological states (e.g. State 1 to State 2 and vice versa [13]).

Appendix A. General Analysis of a Modulated Signal

Any periodically modulated function $g(t)$, with a period 2τ (or frequency $f = 1/2\tau$) can be expressed in terms of a series (Fourier series) of sine and cosine functions, having periods which are whole divisions (1, 2, 3,...,) of the fundamental period 2, i.e.:

$$g(t) = g_o + g_1 \sin\frac{\pi t}{\tau} + g_1' \cos\frac{\pi t}{\tau} + g_2 \sin\frac{2\pi t}{\tau} + g_2' \cos\frac{2\pi t}{\tau} + \ldots + g_j \sin\frac{j\pi t}{\tau} + g_j' \cos\frac{j\pi t}{\tau} + \ldots \quad \text{(A-1)}$$

where the coefficients g_i and g_i' are constants which depend on the function $g(t)$. The term g_0 is the average value of $g(t)$, the next two terms form the fundamental mode, the subsequent two terms give the first harmonic, the two next two terms the second harmonic, and so on for higher harmonics.

In the experimental detection of $g(t)$ by a lock-in-amplifier, it is enough to consider only the fundamental mode. This part of the Fourier series will be denoted here by a squiggle, ~ , above the function:

$$\tilde{g} = I \sin\frac{\pi t}{\tau} + Q \cos\frac{\pi t}{\tau} \quad \text{(A-2)}$$

(where g_1 and g_1' were replaced by the symbols I and Q, respectively). The above two terms of $\tilde{g}$ are the in-phase and quadrature (out-of phase) signals, respectively. The respective coefficients Q and I are the in-phase and quadrature components.

Alternatively, $\tilde{g}$ can be represented equivalently by the amplitude A_S and a phase angle lag ϕ:

$$\tilde{g} = A_S \sin\left(\frac{\pi t}{\tau} - \phi\right) \quad \text{(A-3)}$$

The equivalence of Eqns. A-2 and A-3 leads to the following relations:

$$A_S = \sqrt{I^2 + Q^2} \quad tg\phi = -\frac{Q}{I} \quad \text{(A-4)}$$

The time origin for the above equations is fixed by a reference signal, R, which, by definition, has zero phase angle, i.e.:

$$R = A_R \sin\frac{\pi t}{\tau} \quad \text{(A-5)}$$

R is generated by the lock-in amplifier as a response to an external signal, for example, one which corresponds directly to the intensity of the modulated light (using a fast responding photocell). The true phase angle of R with respect to the modulated light signal can be varied in a controlled manner by a phase adjustment control in the instrument.

A useful visualization of the above terms is by means of a vector diagram. Fig. 1 illustrates this by representing both the fundamental mode of the signal, S, and the reference, R, as (anticlockwise) rotating vectors, each having a constant amplitude and with a common origin. The angular speed of rotation, $\omega (= 2\pi f)$, is constant, and thus the vectors' projections on the fixed y-axis of the usual Cartesian coordinates system produce sinusoidal functions of time. The direction of the reference vector is adjusted so that at $t = 0$ (or at a time of any whole period thereafter) it coincides with the direction of the x-axis. Having a fixed amplitude, A_R, the reference projection on the y-axis, satisfies the same functional dependence as expressed by Eqn. A-5. In order to satisfy Eqn. A-3 the vector representing the fundamental mode of the signal has an amplitude A_S and forms an angle ϕ clockwise to the reference vector. The in-phase and quadrature amplitudes I and Q are represented by the projections of the signal vector on (rotating) orthogonal axes r and s, parallel and perpendicular, respectively, to the reference vector. A phase adjustment is a choice of a new reference vector and therefore a change in the angle ϕ (and hence in I and Q).

The concept shown by the diagram of Fig. 1 is particularly useful for a signal composed of two (or more) independent sinusoidal contributions of equal frequency, as is the case here. The total signal is then represented by a vector which is the vector sum of the vectors representing each contribution separately. The decomposition to in-phase and quadrature vector components on orthogonal axes allows one to add the components of the different contributions separately on each axis.

A1. Calculation of the components of the fundamental mode signal

If $g(t)$ is expressed mathematically as a given function of t, we can find its decomposition in terms of Fourier series components, for the average and fundamental modes, as follows:

$$g_o = \frac{1}{2\tau}\int_0^{2\tau} g(t)\mathrm{d}t$$

$$I = \frac{1}{\tau}\int_0^{2\tau} g(t)\sin\frac{\pi t}{\tau}\mathrm{d}t \qquad \text{(A-6)}$$

$$Q = \frac{1}{\tau}\int_0^{2\tau} g(t)\cos\frac{\pi t}{\tau}\mathrm{d}t$$

Appendix B. Light Saturation Curves of Photosynthesis from Photoacoustic Measurements

We will derive the relation between the photoacoustic signals at various background light intensities and the ordinary light saturation curves of (gross) photosynthesis. Formally, the rate of photosynthesis may be derived by equating the rate of the photochemical conversion of the reaction centers with the rate of their relaxation by secondary electron-transport. This gives an expression for the steady-state concentration of the 'open', active, form of the reaction centers as a function of the (absorbed) light intensity. Substituting back in any one of these two (equal) rate expressions gives then the rate of electron transport.

For Photosystem II, the net rate of the conversion of the reaction centers by light of (absorbed) intensity I may be written:

$$-\frac{\mathrm{d}C}{\mathrm{d}t} = \Phi\cdot\lambda\cdot I\frac{C}{C_t} - k(C_t - C) \qquad \text{(B-1)}$$

where Φ is the quantum yield for charge separation by an active, open, center (the maximum overall quantum yield of photosynthesis), C the concentration of open reaction centers and C_t the total (constant) concentration of all reaction centers. The first term in Eqn. B-1 expresses the rate of photochemical 'closure' (i.e., the reduction of the primary stable acceptor Q, $Q \xrightarrow{h\nu} Q^-$) and the second term the 'reopening' ($Q^- \xrightarrow{k} Q$) by subsequent electron transport with a rate constant k. Eqn. B-1 was made most general, as compared to usual linear models, by introducing an adjustable factor, λ, which depends on C ($\lambda = \lambda(C)$). This factor allows for exciton diffusion over a region of pigments containing more than one reaction center. Generally, $\lambda \to 1$ when $C \to C_t$. (In Joliot's model [14] of energy transfer between closed and open unit λ may be expressed as $\lambda = (1 - p + p[C/C_t])^{-1}$ where p is the energy transfer probability parameter. For the 'independent units' model λ is constant, equal to 1.) To be even more general, one may assume that k itself may also vary with C and/or I. This is because the reoxidation of Q^- may not be strictly first order as it is influenced by the oxidation level of the entity that reacts with Q^-, which is influenced, among other things, by the activity of Photosystem I.

B1. 'Static' response to constant light: rate vs. I relation

We consider the case when a certain constant light intensity I_s is used. A steady state in electron transport is reached, for which case $\mathrm{d}C/\mathrm{d}t = 0$ and hence:

$$\Phi\cdot\lambda_s\cdot I_s\cdot\frac{C_s}{C_t} = k_s(C_t - C_s) \qquad \text{(B-2)}$$

where the subscript s denotes steady-state values). This is an equation for C_s whose solution is:

$$C_s = \frac{k_s C_t^2}{k_s C_t + \Phi\lambda_s I_s} \qquad \text{(B-3)}$$

With regard to the dependence of λ and k on C, this equation may be solved iteratively, at least in principle. For this one assumes the existence of relations $\lambda = \lambda(C)$ and $k = k(C)$. Assuming any arbitrary but plausible initial values for k and λ and after solving for C_s, using Eqn. B-3, new values for λ and k are found which, after resubstitution in Eqn. B-3, lead to a new value of C_s. This process may be continued on and on. It is rapidly convergent (as was checked directly), leading after a few iterations to consistent values of C_s, λ_s and k_s.)

The rate of oxygen evolution in the steady state, r_s, can be obtained from either the left- or right-hand side terms in Eqn. B-2, i.e.:

$$r_s = \Phi \cdot \lambda_s \cdot I_s \frac{C_s}{C_t} \tag{B-4}$$

which after substituting C_s from Eqn. B-3 yields:

$$r_s = \frac{k_s \cdot C_t \cdot \lambda_s \cdot \Phi \cdot I_s}{k_s \cdot C_t + \Phi \cdot \lambda_s \cdot I_s} \tag{B-5}$$

In the following mathematical development we will consider only the restricted case where $\lambda = 1$ and $k =$ constant, particularly since the photoacoustic response vs. I_s, as found here, is consistent with the prediction from this approximation. By this, the derivations become simpler and easy to follow. One may complete the more general derivation, in which case one will have to use the derivatives $d\lambda/dI = (d\lambda/dC) \cdot (dC/dI)$ and dk/dI (e.g., in the computation of dr_s/dI_s).

For the restricted case of $\lambda = 1$, Eqn. B-5 takes the form (writing simply k for the constant k_s)

$$r_s = \frac{k \cdot C_t \cdot \Phi \cdot I_s}{k \cdot C_t + \Phi \cdot I_s} = \frac{r_{max} \cdot \Phi \cdot I_s}{r_{max} + \Phi \cdot I_s} \tag{B-5a}$$

where r_{max} is the asymptotic value of r_s as $I_s \rightarrow \infty$, i.e., $r_{max} = kC_t$.

The 'integral' quantum yield, γ_i, is given from Eqn. B-4 (with $\lambda = 1$) or Eqn. (B-5a) by:

$$\gamma_i = \frac{r_s}{I_s} = \Phi \cdot \frac{C_s}{C_t} = \frac{r_{max} \cdot \Phi}{r_{max} + \Phi \cdot I_s} \tag{B-6}$$

The 'differential' quantum yield, γ_d, is given from Eqn. B-5a by:

$$\gamma_d = \frac{dr_s}{dI_s} = \frac{r_{max}^2 \cdot \Phi}{(r_{max} + \Phi \cdot I_s)^2} \tag{B-7}$$

Note that both integral and differential quantum yields decrease as I_s increases (and tend to zero as $I_s \rightarrow \infty$), the differential yield decreasing much more rapidly. On the other hand, when $I_s \rightarrow 0$ both integral and differential yields tend to the same maximum quantum yield, Φ.

B2. 'Dynamic' response to rapidly varying light intensity

The dynamic response to varying (modulated) light according to Eqn. B-1 is more complicated compared to the previous case, since dC/dt in general is finite and continuously changing. We will assume that the varying intensity of the modulated light, $j(t)$, is sufficiently small so that it can be considered as only a small perturbation around an average point on the ordinary light saturation curve, fixed by (non-modulated) background light of certain intensity (I_s). (Actually one must take I_s to be equal to the background light intensity plus the average of the modulated light intensity.)

The time dependence of the modulated light intensity $j(t)$ (cf. Materials and Methods) consists of alternating off and on half periods, during which the intensity is zero and i, respectively. Each half period has a time duration τ ($= 1/2f$). This pattern may be represented by a combination of an average constant intensity equal to $i/2$ which is to be included as a part of the background light and a true modulated function $j(t)$ expressed as:

$$0 < t < \tau; \quad j = +i/2 \text{ (on period)}$$

$$\tau < t < 2\tau; \quad j = -i/2 \text{ (off period)} \tag{B-8}$$

This function, when developed in a Fourier series (cf. Appendix A), gives the following expression for the fundamental mode of j:

$$\tilde{j}(t) = \frac{2i}{\pi} \sin\frac{\pi t}{\tau} = \frac{2i}{\pi} \sin 2\pi f t \tag{B-9}$$

Eqn. B-1 (with $\lambda = 1$) is rewritten as follows:

$$-\frac{d(C_s + \tilde{C} + \tilde{\tilde{C}})}{dt} = \phi(I_s + \tilde{j} + \tilde{\tilde{j}})\frac{(C_s + \tilde{C} + \tilde{\tilde{C}})}{C_t} - k(C_t - C_s - \tilde{C} - \tilde{\tilde{C}}) \tag{B-10}$$

where $\sim$ symbolizes the fundamental mode, $\approx$ the sum of all higher harmonic terms and the subscript s denotes the constant average value. It is assumed that the amplitude of the modulated light, i, is small enough so that in a power series expansion of $\tilde{C}$ and $\tilde{\tilde{C}}$ as a function of i only the first (linear) term shall be considered *. This assumption is actually required for a unique meaningful

* It is possible to show that this requirement is fulfilled when i is sufficiently small compared with I_s or $k_s C_t/\Phi$. This is always verified in our experiments, even when using weak background light intensities.

interpretation of the photoacoustic measurements, guaranteeing that the ratio of photoacoustic signal to the light intensity is constant, under any given conditions and does not depend on i. In Eqn. B-10 cross terms between $\tilde{j}, \tilde{\tilde{j}}$ and $\tilde{C}$, $\tilde{\tilde{C}}$ have therefore an i^2 dependence and will be ignored. Collecting terms of the same order in i (zero and first orders) and the same basic frequency leads to the following equations for the average and fundamental modes:

$$0 = \Phi \frac{I_s C_s}{C_t} - k(C_t - C_s)$$

(This is the same as Eqn. B-2, with $\lambda = 1$) (B-11)

$$-\frac{d\tilde{C}}{dt} = \Phi \frac{C_s}{C_t}\tilde{j} + \left(\Phi \frac{I_s}{C_t} + k\right)\tilde{C}$$

It is therefore predicted that the average of C, C_s, depends on I_s exactly as in the static case. The fundamental mode of C, $\tilde{C}$, is easily solved by rewriting Eqn. B-11, expressing $\tilde{C}$ in terms of its sine and cosine components with undetermined coefficients, calculating their time derivatives, with $\tilde{j}$ substituted from Eqn. B-9. Equating then separately the sine and cosine terms leads finally to an explicit expression for $\tilde{C}$:

$$\tilde{C} = -\frac{2F}{\pi(4\pi^2 f^2 + F^2)} \cdot \frac{\Phi C_s i}{C_t} \cdot \sin 2\pi ft + \frac{4f}{(4\pi^2 f^2 + F^2)} \cdot \frac{\Phi C_s i}{C_t} \cdot \cos 2\pi ft \qquad \text{(B-12)}$$

where F is an abbreviation for $(k + \frac{\Phi I_s}{C_t})$.

The coefficient of the sine term of $\tilde{C}$ is the in-phase component, relative to $\tilde{j}$, and that of the cosine term is the quadrature component. The quadrature component of $\tilde{C}$ tends to zero at low frequency. To calculate the oxygen-evolution rate we have to use the first term in Eqn. B-1, corresponding to the electron transfer, on the donor side, to the reaction center. (Note that the two rate terms of Eqn. B-1 are not equal in the dynamic case, only their averages are. Note also that the damping factors modify this rate by constant amplitude attenuation and constant phase shift, at any given frequency, and need not be considered specifically.) Hence:

$$r(t) = \frac{\Phi}{C_t}\left[I_s + \tilde{j} + \tilde{\tilde{j}}\right]\left[C_s + \tilde{C} + \tilde{\tilde{C}}\right] \qquad \text{(B-13)}$$

Again, rejecting cross terms between $\tilde{j}, \tilde{\tilde{j}}$ and $\tilde{C}$, $\tilde{\tilde{C}}$ because of i^2 dependence, the fundamental mode for $r(t)$, $\tilde{r}$, is found:

$$\tilde{r} = \frac{\Phi}{C_t} I_s \tilde{C} + \frac{\Phi}{C_t} C_s \tilde{j} \qquad \text{(B-14)}$$

Considering Eqn. B-12 for $\tilde{C}$ it turns out that in the high-frequency limit where $\tilde{C} \to 0$:

$$\tilde{r} = \frac{\Phi}{C_t} C_s \tilde{j} = \frac{r_s}{I_s}\tilde{j} = \gamma_i \tilde{j} \qquad \text{(B-15)}$$

(cf. Eqn. B-4, with $\lambda_s = 1$) i.e., $\tilde{r}$ is proportional to the integral quantum yield.

The 'oxygen-evolution' photoacoustic signal, being proportional to $\tilde{r}$, will have in this case an amplitude proportional to $\gamma_i \cdot i$, as anticipated (cf. main text). It will have a constant phase shift (independent of the background light) arising from the combination all processes starting with the primary photochemical transfer and ending with the final signal. (The photochemical electron-transfer rate is in-phase with respect to the modulated light, as can be seen from Eqn. B-15).

At the low-frequency limit we shall neglect terms depending on f or f^2 in Eqn. B-12. The quadrature term of $\tilde{C}$ is neglected and therefore (considering Eqn. B-9):

$$\tilde{C} = -\frac{\Phi C_s}{F C_t}\tilde{j} \qquad \text{(B-16)}$$

Substituting this expression in Eqn. B-14 yields:

$$\tilde{r} = \left[\frac{\Phi C_s}{C_t} - \frac{\Phi^2 C_s}{F C_t^2} I_s\right]\tilde{j} \qquad \text{(B-17)}$$

The term in the brackets corresponds to the derivative dr_s/dI_s as can be checked by direct differentiation of Eqn. B-4 (with $\lambda_s = 1$) (i.e., $dr_s/dI_s = \Phi[C_s/C_t + I_s/C_t \cdot (dC_s/dI_s)]$ using the expressions for C_s and dC_s/dI_s from Eqn. B-3). Thus, in this case the photoacoustic oxygen evolution signal, being proportional to $\tilde{r}$, is proportional to the differential quantum yield.

For the more general case of variable λ and k, the whole derivation as sketched above must be repeated, with the use of $(\lambda + \tilde{\lambda} + \tilde{\tilde{\lambda}})$ as a multiplier of Φ in Eqn. B-10 and similarly with $(k + \tilde{k} + \tilde{\tilde{k}})$, instead of k. One may use the presumed functional relations $\lambda(C)$ and $k(C)$ to obtain the substitution $\tilde{\lambda} = \frac{d\lambda}{dC}\tilde{C}$ and $\tilde{k} = \frac{dk}{dC}\tilde{C}$. This will result in a correspondingly modified Eqn. B-11. Ultimately, however, the result for the low- and high-frequency limits is the same, as that obtained above, for the simplified case.

We tried also a different procedure, solving Eqn. B-1 directly for the given values of I_s and the function $j(t)$ as in Eqn. B-8. This leads to an expression for C in the form of an exponentially decaying function approaching a steady state (different for the on and off light periods). Developing C in a Fourier series gives then essentially the same result, as obtained above.

References

1 Bults, G., Horwitz, B.A., Malkin, S. and Cahen, D. (1982) Biochim. Biophys. Acta 679, 452–465

2 Rosencwaig, A. (1980) Photoacoustics and Photoacoustic Spectroscopy, Wiley, New York

3 Bults, G., Horwitz, B.A., Malkin, S. and Cahen, D. (1981) FEBS Lett. 129, 44–46

4 Canaani, O., Cahen, D. and Malkin, S. (1982) in Cell Function and Differentiation, Part B (Akoyunoglou, G., Evangelopoulos, A.E., Georgatsos, J., Palaiologos, G., Trakatellis, A. and Tsiganos, C.P., eds.), FEBS Vol. 65, pp. 299–308 Alan R. Liss, New York

5 Kanstad, S.O., Cahen, D. and Malkin, S. (1983) Biochim. Biophys. Acta 722, 182–189

6 Cahen, D. (1982) Rev. Sci. Instrum. 52, 1306–1310

7 Malkin, S. and Cahen, D. (1979) Photochem. Photobiol. 29, 803–813

8 Lasser-Ross, N., Malkin, S. and Cahen, D. (1980) Biochim. Biophys. Acta 593, 330–341

9 Rashevsky, N. (1960) Mathematical Biophysics. Physico-Mathematical Foundation of Biology, Vol. 1, Dover Publications Inc. New York. 1960 edn., 39–47

10 Joliot, P., Hofnung, M. and Chabaud, R. (1966) J. Chim. Phys. 66, 1423–1441

11 Sestak, Z. (1977) in Plant Photosynthetic Production – Manual of Methods (Sestak, Z., Catsky. J. and Jarvis, P.G., eds.), pp. 672–701, Dr. W. Junk, The Hague

12 Malkin, S., Armond, P.A., Mooney, H.A. and Fork, D.C. (1981) Plant Physiol. 67, 570–579

13 Canaani, O., Cahen, D. and Malkin, S. (1982) FEBS Lett. 150, 142–146

14 Joliot, A. and Joliot, P. (1964) C.R. Acad. Sci. Paris 258, 4622–4625